

Microcellular foam of styrene-isobutylene-styrene copolymer (SIBS) with N₂ using polypropylene as a crystallization nucleating and shrinkage reducing agent

Wei yuan Lin, Yuta Hikima, Masahiro Ohshima

Department of Chemical Engineering, Kyoto University, Kyoto 615-8510, Japan

Abstract: Styrene-isobutylene-styrene copolymer (SIBS) is a thermoplastic elastomer with excellent chemical stability, biocompatibility, and low gas permeability. SIBS is a good candidate with a high melt viscosity and a high storage modulus to develop new lightweight elastomeric products. Foam injection molding with core-back operation is an efficient method to prepare SIBS foams. However, it is challenging to prepare a microcellular foam from neat SIBS by melt processing, such as foam extrusion or foam injection molding, because the hard segments cannot play a role in bubble nucleation sites in the molten state. Furthermore, a significant degree of shrinkage occurs after foaming. By introducing a semi-crystalline polymer such as polypropylene (PP), the foamability can be improved in foam injection molding processes. By adjusting the foaming temperature to the crystallization temperature of PP, PP crystals provide bubble nucleation sites and increase the viscosity to suppress bubble growth. Microcellular foams with high cell density and small cell size were achieved at 10^8 cells/cm³ and approximately 13 μ m. PP can also impede the shrinkage of SIBS foams.

1. Introduction

Thermoplastic elastomers (TPEs), including thermoplastic polyurethane (TPU), are block copolymers of an alternating sequence of hard and soft segments. The hard segment can be employed as a physical crosslink site to form a three-dimensional network, and soft segment endows high flexibility. This structure gives TPE an outstanding elastic behavior [1-3] and pronounced processability because of its reversible elasticity with heat [3]. Foaming is a promising method to expand the application of TPE. TPE foams have been used in various fields such as sportswear, automobile parts, packing materials, and medical equipment [4-5]. Chemical foaming has been a central technique for elastomeric foams [6]. However, from the viewpoint of environmental issues, the foaming technique with green physical blowing agents (PBA) such as CO₂ and N₂ and without chemical crosslinking agents will play an essential role in increasing the recyclability of foams. Based on this view, there have been many studies on

the physical foaming processes of TPE and TPU foams. Nofar and his coworkers investigated the effect of hard and soft segment contents on the batch foaming behaviors of TPU [8-9]. They reported that heterogeneous cell nucleation was improved when the hard segment content was higher. The hard segment formed crystal parts and played the role of cell nucleation sites. The high content of the hard segment also broadened the processing window and hindered the shrinkage of the foams. When the molecular weight of the soft segment increased, the expansion ratio increased, while the hard segment controlled the shrinkage. Ge et al. showed that the expansion ratio could be increased by batch foaming with a lower hard segment content, and the crystalline region made from the hard segment could increase the cell density [10]. Ghariniyat and Leung developed a novel TPU-hexagonal boron nitride composite foam with an improved thermal conductivity using a batch foaming method. They demonstrated that the formation of a thermally conductive filler network in foams could be promoted by the synergy of the post-foaming elastic recovery and foam-induced filler alignment [11]. Shabani and coworkers conducted batch foaming, foam extrusion, and bead foam of TPU and compared the cell structures of the resulting foams. Their results show that the foams produced by batch foaming had a higher cell density and a smaller cell size than foam extrusion and bead foaming [12]. Qu and his coworkers investigated batch foaming of a blend of polystyrene and TPU. They reported that the solubility of CO₂ and the rheological properties were enhanced by blending PS with TPU, and a bimodal cellular structure was formed by blending TPU with PS as a dispersed domain [13]. Wang and his coworkers studied the effect of elastic strain energy on the TPU cell nucleation and found that both stretching and compression could facilitate cell nucleation where stretching was much more efficacious [14]. As reviewed, most of the research on TPE or TPU physical foaming was conducted by batch foaming or bead foaming methods, where the presence of hard and soft segments can be used effectively to control the cell structure.

The foam injection molding technique is attractive for foaming thermoplastic polymers in general because of the short cycle time, less material usage, and higher dimensional stability of the foams [7, 15, 16, 17]. However, the traditional foam injection molding (FIM) with short-shot and full-shot methods have several issues. For example, cell nucleation and cell growth are restricted, especially in the short-shot method. The expansion ratio and weight reduction are low (usually less than 30%), which hinders the applications of injection-molded foam products. Furthermore, the high melt temperature and strong shear flow during the injection stage deteriorate the cell structure, so foam products may suffer poor functionality [7, 18-19].

To overcome these shortcomings, the core-back foam injection molding technique or precise mold opening technique has been applied to thermoplastic polymers. The technique significantly improves the cellular structure and mechanical properties, and it can fabricate high-expansion foams. Wang prepared a lightweight polyether block amide (PEBA) foam with excellent elasticity and thermal-sound insulation properties using core-back foam injection molding technology [20]. Ellingham et al. extended core-back foam injection molding to a three-stage microcellular injection molding technique. They produced lightweight TPU foams with various densities, cell structures, and mechanical properties [21].

Poly(styrene-block-isobutylene-block-styrene) (SIBS) is a TPE composed of a hard styrene segment and a soft isobutylene segment. Compared with other TPEs or TPUs, it is gaining significant attention in biomedical applications because of its high biocompatibility [22, 23]. In addition, it exhibits excellent heat aging resistance, superior gas barrier-ability, and damping behavior, so it is promising for many applications [24]. However, it remains difficult to prepare any foams from neat SIBS by melt processing with a uniform fine cell structure. Polymer blending or the addition of a filler is a simple and effective method to improve the physical properties of SIBS [25-27].

In this study, polypropylene was used to improve the cell structure and foamability of SIBS. PP is a semi-crystalline polymer, and its crystallization behavior can play the role of a cell nucleating agent and improve the foamability with CO₂ or N₂, as shown in thermoplastic polymer foaming [28-29]. SIBS/PP with 10%, 20%, and 30% PP contents were fabricated by the core-back injection molding technique, and the effects of PP on SIBS foaming and the shrinkage of the foams were investigated. The crystallization rate, rheology, and morphology of SIBS/PP were evaluated to clarify the effects.

2. Experimental

2.1. Materials. Styrene-isobutylene-styrene block copolymer (SIBS073T, Kaneka, Osaka, Japan) with a 6.0 g/10 min (230 °C/2.16 kg) melt flow rate was provided and used as is. Polypropylene (Waymax MFX3, Japan Polypropylene Corporation, Tokyo, Japan) with an 8.0 g/10 min (230 °C/2.16 kg) melt flow rate was used as a viscosity modifier, cell nucleating agent, and shrinkage prohibiting agent. Nitrogen (N₂, Izumi Sanyo, Tokyo, Japan) was utilized as a physical blowing agent (PBA) with a purity over 99%.

2.2. Sample preparation. A 35-ton clamping force MuCell® foam injection molding machine

(J35EL III-F, Japan Steel Work, Hiroshima, Japan) and a gas delivery system (SCF device SII TRJ-10-A-MPD, Trexel Inc., USA) were used. N₂ was pressurized to 24 MPa by the gas delivery system and injected into the molten polymer in the barrel of the injection molding machine through an injector valve. The N₂ concentration in the polymer was set at 0.1% by manipulating the valve opening period of the injector valve. Mixing the gas with molten polymer at higher temperatures and pressures with a screw enhances the gas dispersion and dissolution and creates a single-phase N₂/polymer solution. The temperatures of the injection molding machine were set at 150, 180, 200, 200, 200, 200, and 200 °C from the bottom of the hopper (feeding zone) to the shut-off nozzle (nozzle zone). The mold temperature was maintained at 40 °C. The mold has a rectangular cavity with dimensions of 70 mm × 50 mm × 2 mm. The temperature and pressure sensor locations were given in our previous paper [30]. The experimental conditions are summarized in Table 1.

Table 1 Experimental conditions for the injection molding machine.

Parameters	Values
PP content wt.%	0, 10, 20, 30
Temperature (°C)	150, 180, 200, 200, 200, 200, 200
Mold temperature (°C)	40
Injection speed (mm/s)	100
Screw back pressure (MPa)	15
Dwelling time (s)	7-11.5
Core-back distance (mm)	2
Core-back speed (mm/s)	20
Metering distance (mm)	50
N ₂ content (%)	0.1

2.3. Thermal analysis. Fast scanning chip calorimetry (FSC) was conducted using Mettler-Toledo Flash DSC1 (Mettler-Toledo, LLC, USA) to observe the non-isothermal crystallization behavior of PP in the blend polymers. Thin films of SIBS and SIBS/PP blends 10–20 μm in thickness were prepared by hot compression at a temperature of 200 °C under 30 MPa mechanical pressure. A small piece specimen was cut out from the thin films and used for measurement. Fig. 1a shows a temperature profile of the polymer injected into the mold cavity. The temperature profile was divided into several time zones, and a constant cooling rate was assumed in each zone. The temperature change of Flash DSC was programmed as shown in Fig. 1b by simulating the cooling temperature profile: the temperature was first increased to 200 °C at 1000 °C/s. Then, it was decreased at the constant cooling rates associated with the cooling rate of the time zones. Immediately after reaching the end temperature of the designated

number of zones, the temperature was rapidly increased to 200 °C at 1000 °C/s, and the heating curve was obtained. The procedure was repeated by extending the number of zones one by one in the FSC cooling process. The onset of crystallization in the cooling process shown in Fig. 1a was estimated from the heating curve, where a melting peak first appeared.

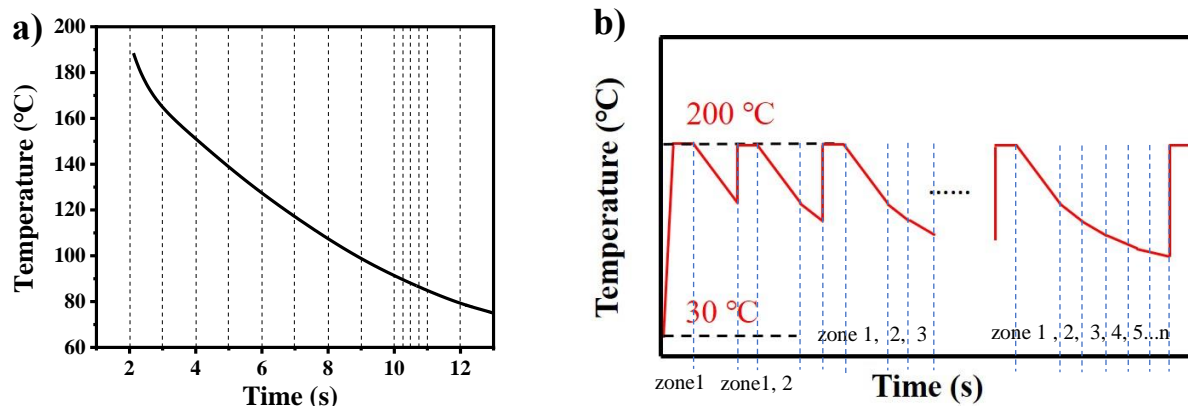


Fig. 1. a) A temperature profile of the cooling process in the mold cavity; b) the specific FDSC program of the discrete method for determining the onset and the maximum crystallization rate temperatures during the rapid cooling process.

2.4. Rheological characterization. Strain-controlled frequency sweep and temperature ramp sweep measurements were conducted using an ARES rheometer with a 25-mm parallel-plate device. The specimens were prepared 25 mm in diameter and 2 mm in thickness using a hot compressing machine at a temperature of 200 °C and compression pressure of 10 MPa. Frequency sweep measurements were conducted in the frequency range of 0.1-100 rad/s with a 1% strain amplitude at 200 °C. Temperature sweep measurements were conducted in the range of 100–200 °C with a 1% strain amplitude and 0.63 rad/s. The damping rate was 2 °C/min.

2.5. Blend morphology observation. The blend morphology of SIBS/PP was observed by a scanning electron microscope (FE-SE) (JSM-6340F, JEOL Ltd., Tokyo, Japan). All specimens were cut out from the middle parts of the nonfoamed injection-molded products after cryogenically fracturing in liquid nitrogen. Prior to the SEM observation, RuO₄ was used to differentiate the SIBS matrix and PP domains [31-33]. Then, after three hours of staining, the stained sample was dried in vacuo for at least 6 hours.

2.6. Cell structure characterization. The cell structure of the foams was evaluated by the cell size and cell density. The cell structure was investigated using a scanning electron microscope (Tiny-SEM Mighty-8, Technex, Tokyo, Japan). A small slice specimen was cut from the center of the injection-molded product and cryogenically fractured in liquid nitrogen. The fractured

surface was gold-coated using a quick coater (VPS-020, ULVAC KIKO, Ltd., Japan). Then, SEM images were analyzed using ImageJ (National Institutes of Health, USA). The cell density (N_0) was calculated by Eq. (1), and over 200 cell diameters were measured and averaged in Eq. (2) [34-35]:

$$N_0 = \left(\frac{n}{A}\right)^{\frac{3}{2}} \quad (1)$$

where n is the number of cells chosen in the designated SEM image area, and A is the selected area in the image. The average cell diameter can be obtained by equation (2) [5]:

$$d = \frac{\sum d_i n_i}{\sum n_i} \quad (2)$$

where n_i is the number of bubbles (pores) with diameter d_i , assuming that the bubble is spherical.

2.7. Shrinkage evaluation. The foam shrinkage ratio was calculated from the foam density. The foam density was measured by an electronic densimeter (MDS-300, Alfa Mirage Co., Ltd, Japan) every day after the foam injection molding for 35 days. Then, the shrinkage ratio was given by

$$\text{Shrinkage Ratio} = 1 - \frac{\rho_{\text{foam}_1}}{\rho_{\text{foam}_n}} \quad (3)$$

where ρ_{foam_1} is the foam density immediately after the foam injection molding, and ρ_{foam_n} is the foam density from day 2 ($35 \geq n \geq 2$).

2.8. Compression test. The mechanical properties of SIBS-based foams were investigated by using a universal testing machine (Autograph AGS-1kN, Shimazu, Japan) with a compression speed of 1 mm/min. The rectangular-shaped specimen was prepared by cutting the middle of injection-molded nonfoamed products. Four specimens were tested and averaged for each condition.

3. Results and conclusions

3.1. Rheological analysis. Fig. 2 shows the frequency versus storage modulus (G') and complex viscosity (η^*) of neat PP, neat SIBS, and their blends with three different blend ratios. As shown in Fig. 2(a), G' of neat PP exhibited terminal flow behavior in the low-frequency range [36-37], and G' of SIBS/PP blends decreased with increasing PP content in the entire frequency region, since the SIBS matrix softened with minor PP domains. A plateau was observed in the low-frequency range of neat SIBS and SIBS/PP blends, which is called the

pseudo-solid-like behavior. This behavior indicates the existence of a network-like structure [26]. The G' value in the plateau region reflects the level of network formation, and the level decreased when the PP content increased. η^* of PP reached a Newtonian plateau in the low-frequency range, and all polymers showed shear-thinning behaviors in the high-frequency range, as shown in Fig. 2b.

Fig. 3 shows Han's plot of neat PP, neat SIBS, and their blends. As shown in Fig. 3, neat PP showed a linear relationship between G' and G'' , while neat SIBS and SIBS/PP blends showed nonlinear correlations. The nonlinear behavior of neat SIBS indicates a microdomain structure of block polymer in neat SIBS, and the nonlinear correlation of blends with different slopes indicates immiscibility and incompatibility between PP and SIBS. It can be speculated that the PS hard segment of SIBS forms the network structure at the experimental temperature (200 °C). The order-disorder transition temperature of SIBS, where the microdomain structure disappears and becomes a homogenous phase, was reported to be higher than 250 °C [38-40].

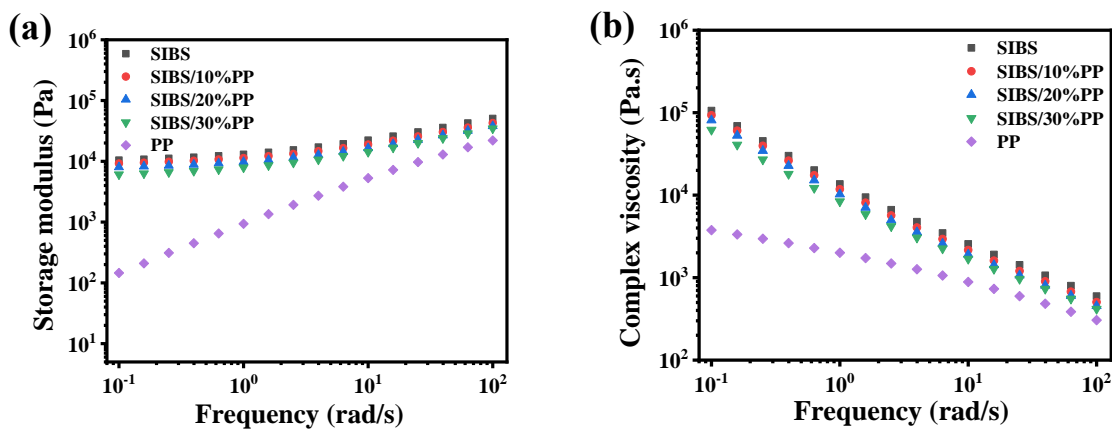


Fig. 2. Frequency sweep test: (a) Storage modulus (G'); (b) complex viscosity (η^*) (200 °C).

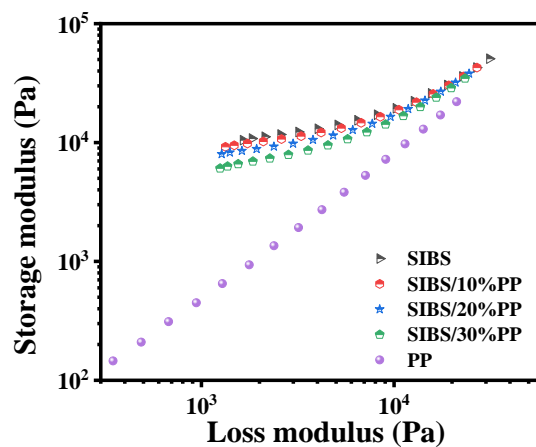


Fig. 3. $G' \sim G''$ Han's plots (200 °C).

Fig. 4 shows the SEM images of the non-foamed injection-molded SIBS and SIBS/PP

blend morphologies. The black domains represent PP, and the white is the SIBS matrix. Fig. 4 illustrates that PP and SIBS were immiscible and incompatible, as the rheological analysis indicated, and the black domains increased with increasing PP content. The fiber-like shaped black domains were observed in the blends, which is attributed to the shear flow induced by injection.

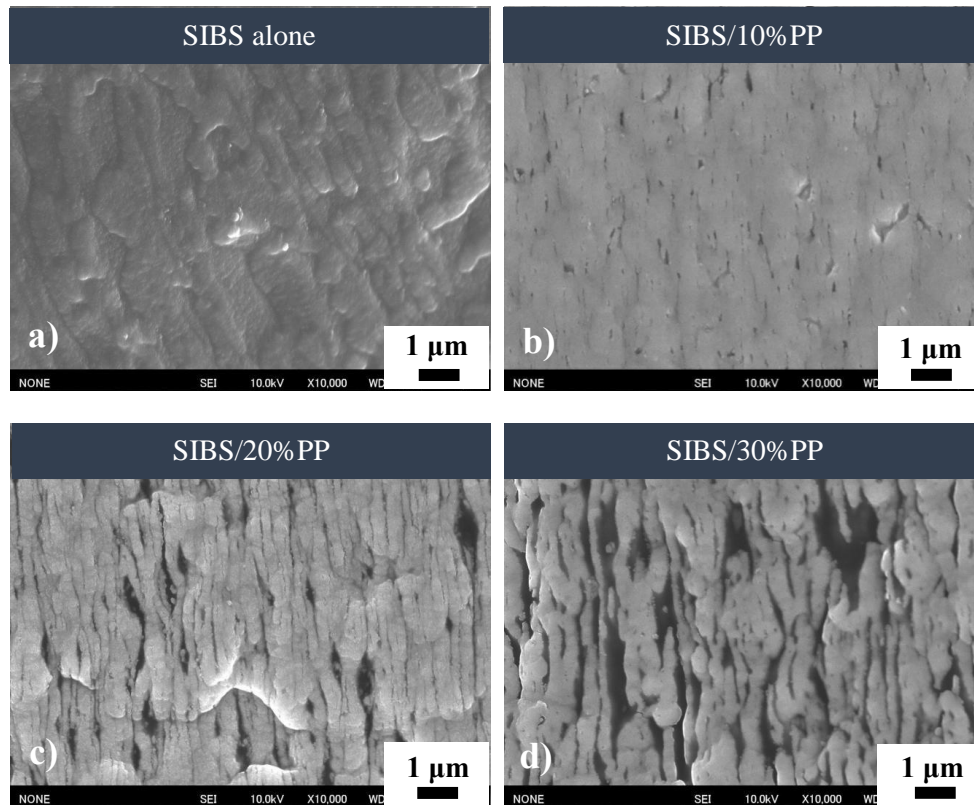


Fig. 4. SEM images of blend morphology stained with RuO₄: a) SIBS, b) SIBS/10% PP, c) SIBS/20% PP and d) SIBS/30% PP.

Fig. 5 shows the temperature dependency of η^* of neat PP, neat SIBS, and blends. The η^* values of SIBS and the blends were higher than 10^4 Pa over the entire temperature range, which indicates that a rubber-like behavior exists and is insensitive to temperature. The η^* values decreased when the PP content increased; when the PP content exceeded 20 wt.%, a notable viscosity change occurred at a temperature of approximately 135 °C. The degree of change increased when the PP content increased. These temperature sweep tests demonstrated that crystallization of PP occurred in SIBS/PP blends.

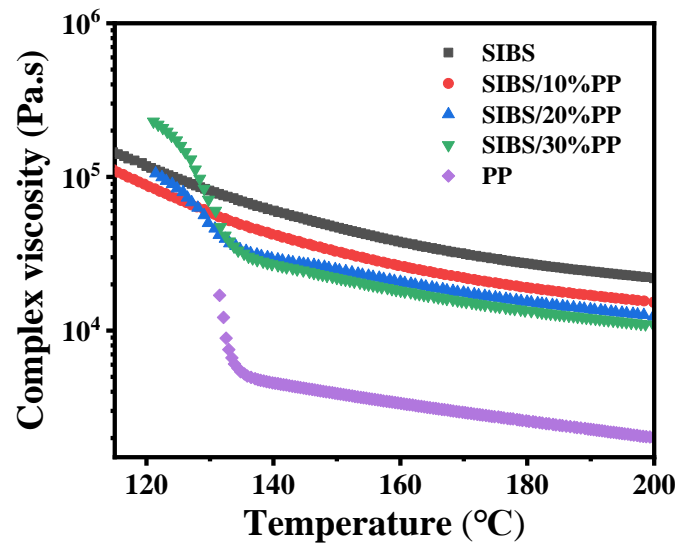


Fig. 5. Complex viscosity of SIBS-based materials in the range from 115 to 200 °C.

3.2. Flash DSC analysis. The rheological analysis based on temperature sweep tests indicates that the crystallization of PP occurs in SIBS/PP blends. Growing crystals can be used as an effective bubble nucleating agent in the foaming process [28, 41-42]. The discrete thermal analysis method using Flash DSC with the temperature program illustrated in Fig. 1b was helpful to observe that the crystallization of PP occurs in a rapid cooling process of the foam injection molding process. Figs. 6a and 6b show the heating curves of SIBS/PP (20 wt.%) and SIBS (30 wt.%). Unfortunately, the heat of fusion was too small to be detected in the heating curves of SIBS/PP (10 wt.%). In Fig. 6, the legend of both figures indicates the temperature at which heating began after a cooling process of Flash DSC, which consisted of the designated number of zones. For SIBS/PP (20 wt.%), a melting peak appeared in the heating curve after the temperature decreased to 95.5 °C or lower, while no noticeable peak was observed in the heating curve after cooling until the temperature below 97.9 °C. Thus, it can be estimated that the crystallization of PP in SIBS/PP (20 wt.%) occurred when the temperature dropped into the range of 95.5-97.9 °C during the rapid cooling process. For SIBS/PP (30 wt.%), crystallization occurred when the foaming temperature decreased to 98.4-101.7 °C in the rapid cooling process.

Fig. 7 shows the heat of fusion measured from the heating curves, which clearly indicates the onset of PP crystallization when the temperature decreased to 95-98 °C for SIBS/PP (20 wt.%) and 98-100 °C for SIBS/PP (30 wt.%). The discrete method results were used to analyze the effect of PP crystals in the blended polymers on the cellular structure. Furthermore, the discrete method shows that the peak of crystallization rate against the temperature was estimated from the ΔH -temperature curves inflection points and was located

at approximately 85 °C for SIBS/PP (20 wt.%) and 88 °C for SIBS/PP (30 wt.%).

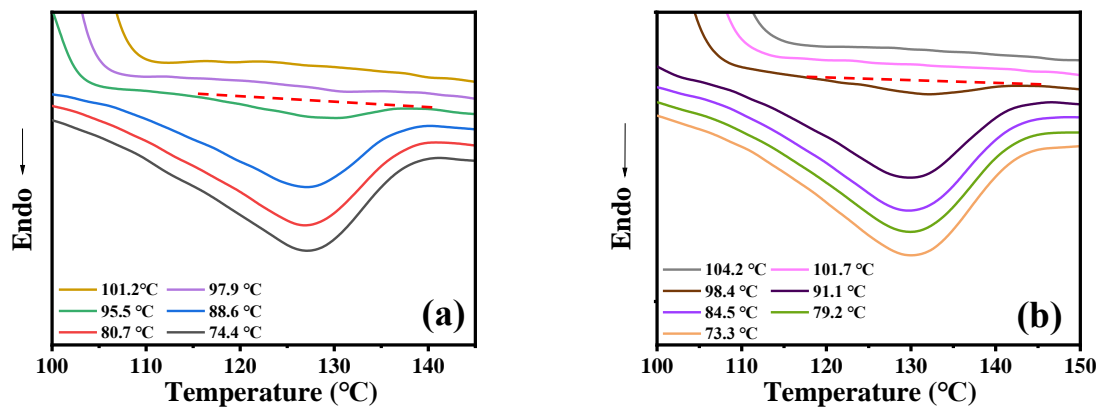


Fig. 6. Heating curves of SIBS/20%PP (a) and SIBS/30%PP (b) cooled down to the different cooling temperatures along a rapid cooling temperature profile in mold.

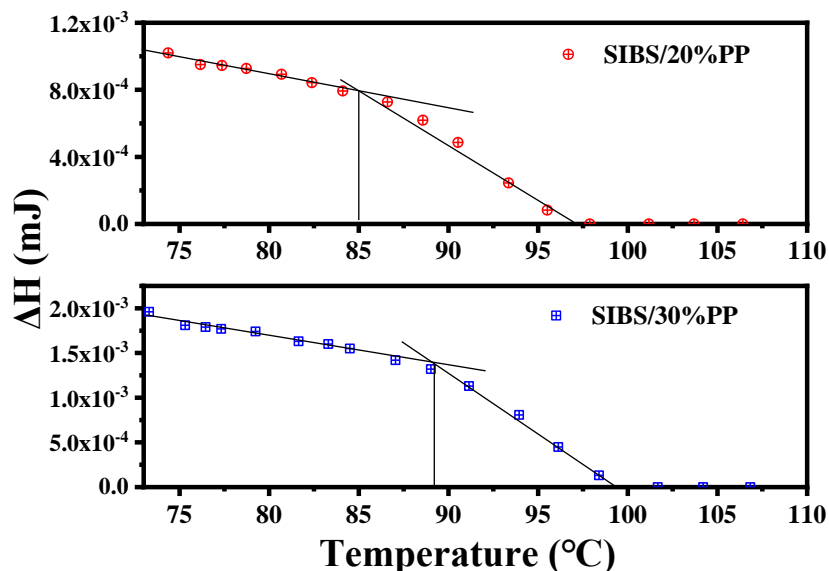
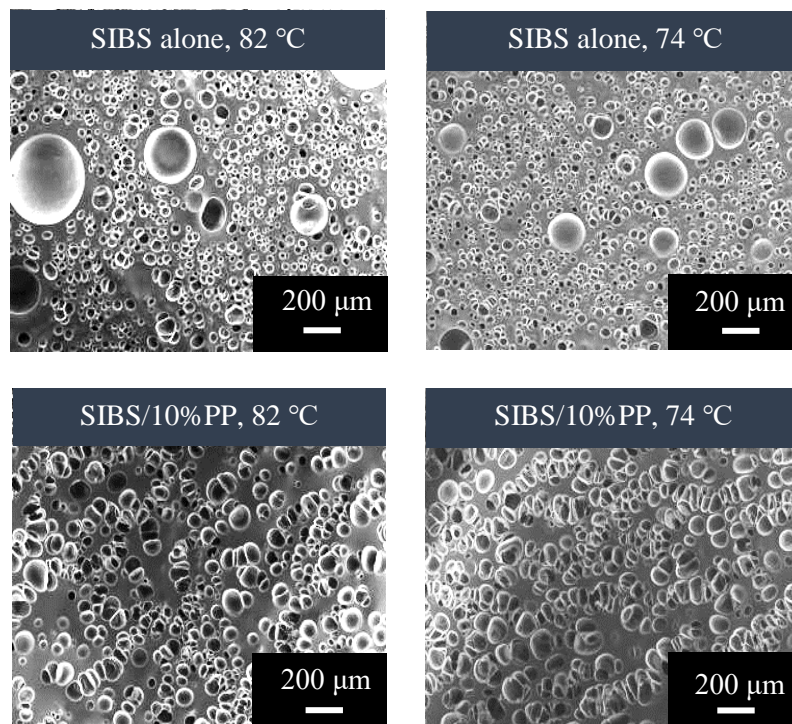


Fig. 7. Heat of fusion, ΔH , of SIBS/20%PP and 30%PP crystallized by cooling down to the temperature along the cooling temperature profile of Fig. 1a.

3.3. Effects of PP blending on cell structure. Figs. 8 and 9 show the SEM images of the cell structure of the 2-fold expansion foams prepared at various foaming temperatures. The images were taken from the view perpendicular to the core-back direction. The foaming temperature was the temperature at which the core-back operation commenced. As shown in Fig. 8, the cell size decreased when the foaming temperature decreased in both neat SIBS and the blend foams. However, the neat SIBS foams had a few large bubbles and fewer tiny bubbles even at the lower foaming temperature, while the blend polymer foams showed a relatively uniform

microcellular structure with more bubbles. Thus, PP provides bubble nucleation sites and increases the number of bubbles.

Fig. 9 shows the SEM images of the SIBS/PP (20 and 30 wt.%) foams prepared with foaming temperatures of 94 and 99 °C for SIBS/20% PP, and 97 and 100 °C for SIBS/30% PP. These images indicated the PP crystallization effect on the cell structure: The cellular structure of blends was changed by decreasing the foaming temperature to below the onset temperature of PP crystallization in the rapid cooling process. At the foaming temperatures higher than 98 °C, PP was not crystallized when foaming was conducted by a core-back operation. Instead, it provided not only the lower viscosity but also inhomogeneous viscosity domains in the injected polymers and caused the non-uniformity of cell morphology with larger bubbles. However, at the foaming temperatures below 97 °C, the PP domains started crystallization and they provided the bubble nucleation sites. As a result, the cell size became smaller and the uniformity of cell morphology increased.



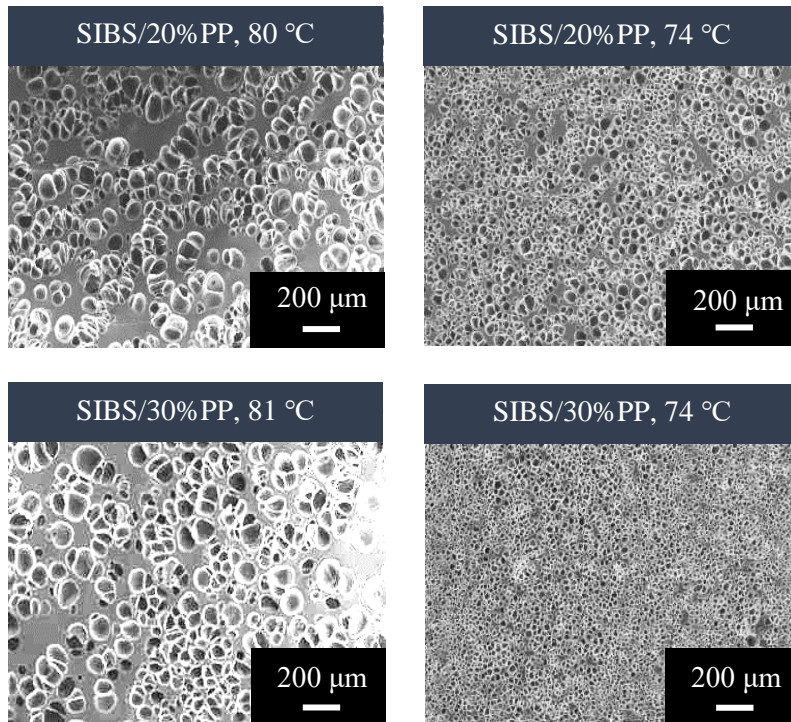


Fig. 8. SEM images of the cell structure of SIBS and SIBS/PP blend foams prepared at different foaming temperatures.

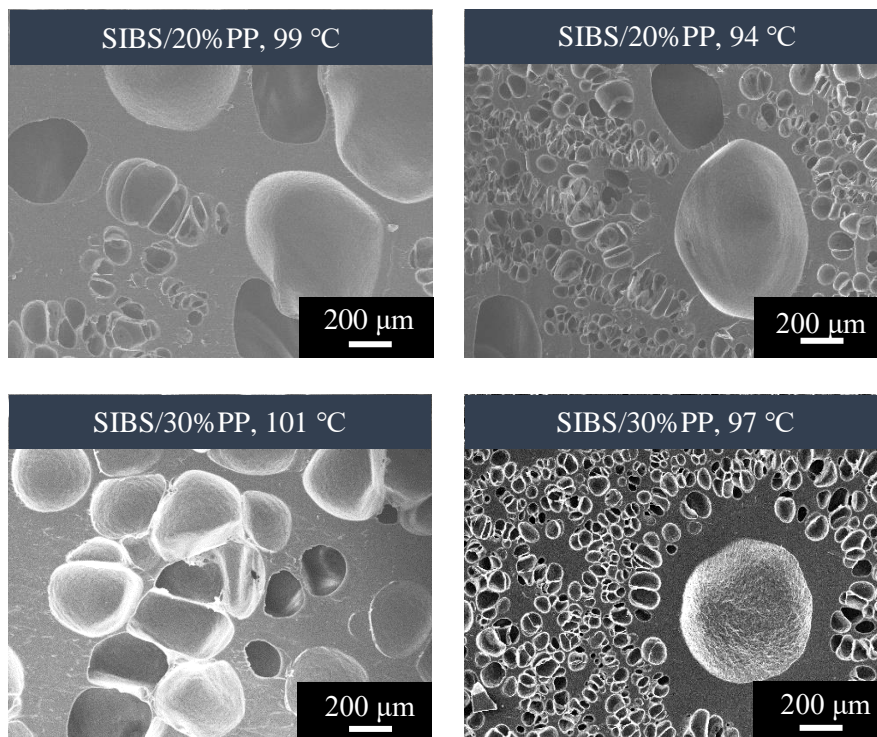


Fig. 9. SEM images of SIBS/20% and 30%PP at higher foaming temperatures (94 and 99 °C for SIBS/20%PP, 97 and 101 °C for SIBS/30%PP).

Fig. 10 shows the cell density and cell diameter estimated from the SEM images of the foams. The cell densities of SIBS/PP blend foams were drastically increased by lowering the foaming temperature. The cell density began to increase at a higher foaming temperature with increasing PP content in the blend. The degree of increase in cell density also increases with increasing PP content.

Regarding the cell size, the neat SIBS foam shows smaller cell diameters at the entire foaming temperature. Blending PP could not decrease the cell diameter at foaming temperatures above 79 °C for SIBS/PP (30 wt.%) and 76 °C for SIBS/PP (20 wt.%). The cell diameter of the SIBS/PP (10 wt.%) foam did not decrease compared to that of the neat SIBS foams at all foaming temperatures. The effect of PP on the cell size was attributed to the rheological effect of PP. The viscosity decreased with increasing PP content, as shown in Fig. 2. When and if the higher viscosity of PP is used for blending, the cell size may decrease with increased PP content in the blend. It is commonly observed in the microcellular foaming when the viscosity increases, the cell size decreases and the cell density increases because the higher viscosity can suppress the bubble growth. However, in the SIBS/PP blends case, the viscosity decreased, and the cell size decreased, but the cell density increased with PP. Fig.10 indicates that PP increases bubble nucleation sites to SIBS despite decreasing the viscosity.

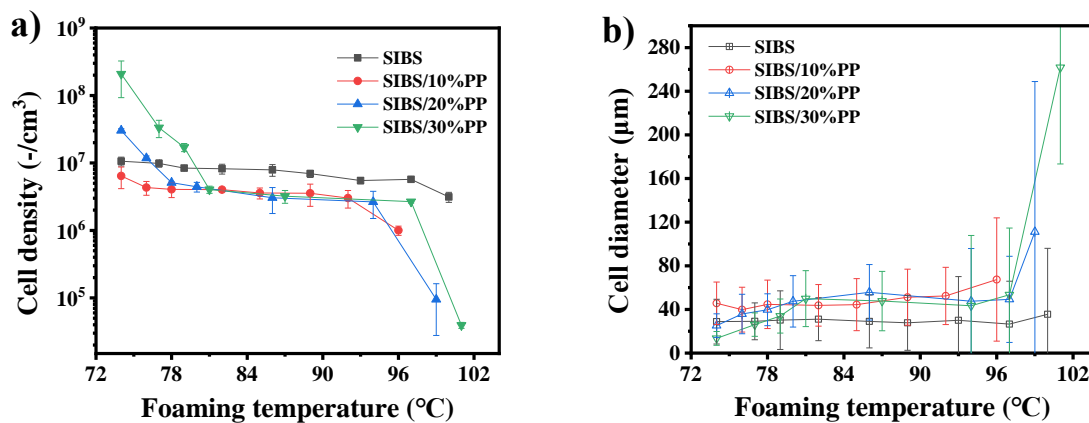


Fig. 10. Change in cell density and cell diameter of SIBS and SIBS/PP blend foams against foaming temperature.

3.4. Shrinkage evaluation. As described in the introduction, shrinkage is one of the critical issues of TPE and TPU foaming. Shrinkage occurs when the residual blowing agent diffuses out from the foam. Fig. 11 shows the shrinkage ratio of neat SIBS and SIBS/PP blend foams prepared at 74 °C foaming temperature. The shrinkage can be impeded by PP blending. When

the PP content increased, the anti-shrinkage effect of PP became more pronounced. The effect is attributed to the increase in gas permeability of SIBS and increase in modulus due to PP.

Fig. 12 shows the compression data of SIBS and SIBS/PP blends. SIBS with a higher PP content showed a higher compression modulus. The modulus was enhanced when the PP content increased due to the increase in PP crystallinity. The higher compression modulus acts as a resistance to deformation and shrinkage [43].

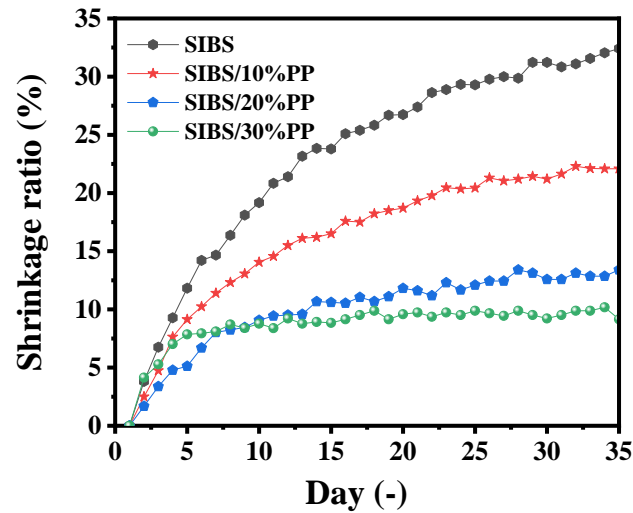


Fig. 11. Change in shrinkage ratio of the foams with different PP contents throughout the day.

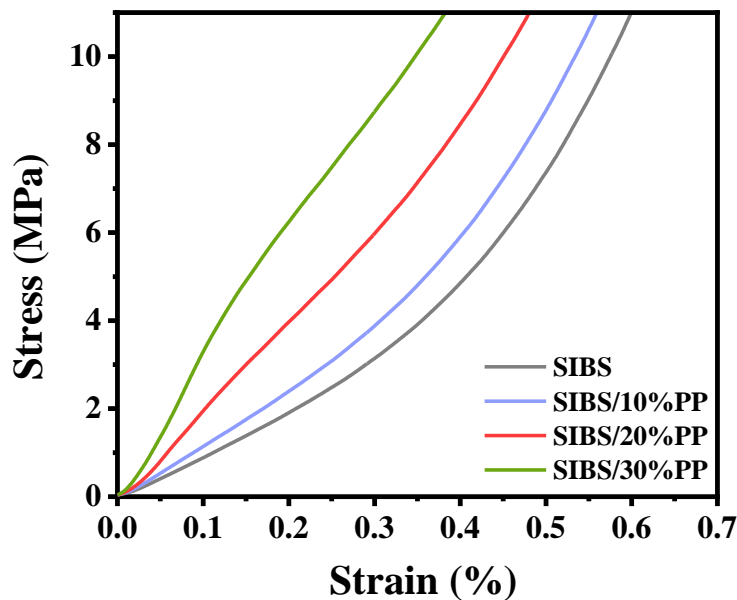


Fig. 12. Compression vs. strain curve of SIBS and SIBS/PP blends.

4. Conclusion

In this study, neat SIBS and SIBS/PP blend foams were prepared by foam injection molding with the core-back operation, and the effect on the cellular structure was investigated. The neat SIBS foams showed a relatively poor uniform cellular structure and a higher shrinkage ratio. The cell density and anti-shrinkage of the foams were drastically improved by blending PP. PP crystals can provide bubble nucleation sites at a lower foaming temperature than the onset of crystallization temperature in the rapid cooling process of the foam injection molding process. Blending PP restrained the shrinkage of SIBS foam after foaming. The blending of semi-crystalline polymers such as PP offers an effective method to improve the cell structure and anti-shrinkage characteristic of amorphous TPE.

Reference

- [1] Drobny, J. G. *Handbook of Thermoplastic Elastomers*, William Andrew Inc.: New York, 2007.
- [2] Shanks, R.; Kong, I. *Thermoplastic Elastomers*; El-Sonbati, A. Z., Ed.; Intech Open: Rijeka, 2012.
- [3] Spontak, R. J.; Patel, N. P. Thermoplastic Elastomers: Fundamentals and Applications, *Curr. Opin. Colloid. Interface Sci.* 2000, 5, 334–341.
- [4] Kong, H. J.; Lee, S. H.; Kim, D. G.; Kim, H. J.; Park, G. W.; Hyun, K. Investigation of Thermoplastic Elastomer (TPE) Foaming Process Using Blowing Agent by Rheological and Morphological Methods. *J. Appl. Polym. Sci.* 2019, 136, 47358.
- [5] Kharbas, H. A.; Ellingham, T.; Manitiu, M.; Scholz, G.; Turng, L. S. Effect of A Cross-Linking Agent on the Foamability of Microcellular Injection Molded Thermoplastic Polyurethane. *J. Cell. Plast.* 2017, 53, 407–423.
- [6] Meng, L. H.; Liu, H. S.; Yu, L.; Khalid, S.; Chen, L.; Jiang, T. Y.; Li, Q. L. Elastomeric Foam Prepared by Supercritical Carbon Dioxide. *J. Appl. Polym. Sci.* 2017, 134, 44354.

- [7] Zhai, W. T.; Jiang, J. J.; Park, C. B. A Review on Physical Foaming of Thermoplastic and Vulcanized Elastomers. *Polym Rev.* 2022, 62, 95–141.
- [8] Nofar, M.; Küçük, E. B.; Batı, B. Effect of Hard Segment Content on the Microcellular Foaming Behavior of TPU Using Supercritical CO₂. *J. Supercrit. Fluids* 2019, 153, 104590.
- [9] Nofar, M.; Batı, B.; Küçük, E. B.; Jalali, A. Effect of Soft Segment Molecular Weight on the Microcellular Foaming Behavior of TPU Using Supercritical CO₂. *J. Supercrit. Fluids.* 2020, 160, 104816.
- [10] Ge, C. B.; Wang, S. P.; Zheng, W. G.; Zhai, W. T. Preparation of Microcellular Thermoplastic Polyurethane (TPU) Foam and Its Tensile Property. *Polym. Eng. Sci.* 2018, 58, E158–E166.
- [11] Ghariniyat, P.; Leung, S. N. Development of Thermally Conductive Thermoplastic Polyurethane Composite Foams via CO₂ Foaming-Assisted Filler Networking. *Compos. B. Eng.* 2018, 143, 9–18.
- [12] Shabani, A.; Fathi, A.; Erlwein, S.; Altstädt, V. Thermoplastic Polyurethane Foams: From Autoclave Batch Foaming to Bead Foam Extrusion. *J. Cell. Plast.* 2021, 57, 391–411.
- [13] Qu, Z. J.; Mi, J. G.; Jiao, Y.; Zhou, H. F.; Wang, X. D. Microcellular Morphology Evolution of Polystyrene/Thermoplastic Polyurethane Blends in the Presence of Supercritical CO₂. *Cell. Polym.* 2019, 38, 68–85.
- [14] Wang, G. L.; Zhao, J. C.; Yu, K. J.; Mark, L. H.; Wang, G. Z.; Gong, P. J.; Park, C. B.; Zhao, G. Q. Role of Elastic Strain Energy in Cell Nucleation of Polymer Foaming and Its Application for Fabricating Sub-Microcellular TPU Microfilms. *Polymer* 2017, 119, 28–39.
- [15] Di Maio, E.; Kiran, E. Foaming of Polymers with Supercritical Fluids and Perspectives on the Current Knowledge Gaps and Challenges. *J. Supercrit. Fluids* 2018, 134, 157–166.
- [16] Xu, J. Y. *Microcellular Injection Molding*, John Wiley & Sons Ltd.: New Jersey, 2010.
- [17] Gong, S.; Yuan, M.; Chandra, A.; Kharbas, H.; Osorio, A.; Turng, L. S. Microcellular Injection Molding. *Int. Polym. Proc.* 2005, 20, 202–214.
- [18] Yang, C. X.; Wang, G. L.; Zhao, J. C.; Zhao, G. Q.; Zhang, A. M. Lightweight and Strong Glass Fiber Reinforced Polypropylene Composite Foams Achieved by Mold-Opening Microcellular Injection Molding. *J. Mater. Res. Technol.* 2021, 14, 2920–2931.

- [19] Shaayegan, V.; Wang, G. L.; Park, C. B. Study of the Bubble Nucleation and Growth Mechanisms in High-Pressure Foam Injection Molding Through In-Situ Visualization. *Eur. Polym. J.* 2016, 76, 2–13.
- [20] Wang, G. L.; Zhao, G. Q.; Dong, G. W.; Mu, Y.; Park, C. B.; Wang, G. Z. Lightweight, Super-Elastic, and Thermal-Sound Insulation Bio-Based PEBA Foams Fabricated by High-Pressure Foam Injection Molding with Mold-Opening. *Eur. Polym. J.* 2018, 103, 68–79.
- [21] Ellingham, T.; Kharbas, H.; Manitiu, M.; Scholz, G.; Turng, L. S. Microcellular Injection Molding Process for Producing Lightweight Thermoplastic Polyurethane with Customizable Properties. *Front. Mech. Eng.* 2018, 13, 96–106.
- [22] Pinchuk, L.; Wilson, G. J.; Barry, J. J.; Schoephoerster, R. T.; Parel, J. M.; Kennedy, J. P. Medical Applications of Poly (Styrene-Block-Isobutylene-Block-styrene) (“SIBS”). *Biomaterials* 2008, 29, 448–460.
- [23] Fittipaldi, M.; Rodriguez, L. A.; Grace, L. R. The Effect of Water Absorption on the Viscoelastic Properties of Poly (Styrene-Block-Isobutylene-Block-Styrene) for Use in Biomedical Applications. *AIP Conf. Proc.* 2015, 1664, 030003-1–030003-5.
- [24] Koshimura, K.; Sato, H. Application Study of Styrene-Isobutylene-Styrene Block Copolymer as a New Thermoplastic Elastomer. *Polym. Bull.* 1992, 29, 705–711.
- [25] Ahmed, M. F.; Li, Y.; Yao, Z.; Cao, K.; Zeng, C. C. TPU/PLA Blend Foams: Enhanced Foamability, Structural Stability, and Implications for Shape Memory Foams. *J. Appl. Polym. Sci.* 2019, 136, 47416.
- [26] Huang, A.; Peng, X. F.; Turng, L. S. In-Situ Fibrillated Polytetrafluoroethylene (PTFE) in Thermoplastic Polyurethane (TPU) via Melt Blending: Effect on Rheological Behavior, Mechanical Properties, and Microcellular Foamability. *Polymer* 2018, 134, 263–274.
- [27] Li, X. Y.; Wang, G. L.; Yang, C. X.; Zhao, J. C.; Zhang, A. M. Mechanical and EMI Shielding Properties of Solid and Microcellular TPU/Nanographite Composite Membranes. *Polym. Test.* 2021, 93, 106891.
- [28] Sharudin, R. W. B.; Nabil, A.; Taki, K.; Ohshima, M. Polypropylene-Dispersed Domain as Potential Nucleating Agent in PS and PMMA Solid-State Foaming. *J. Appl. Polym. Sci.* 2011, 119, 1042–1051.
- [29] Banerjee, R.; Ray, S. S. Foamability and Special Applications of Microcellular

Thermoplastic Polymers: A Review on Recent Advances and Future Direction. *Macromol. Mater. Eng.* 2020, 305, 2000366.

[30] Ishihara S., Hikima, Y.; Ohshima, M. Preparation of Open Microcellular Poly(lactic Acid) Foams with a Microfibrillar Additive Using Coreback Foam Injection Molding Processes. *J. Cell. Plast.* 2018, 54, 765–784.

[31] Trent, J. S.; Scheinbeim, J. I.; Couchman., P. R. Ruthenium Tetraoxide Staining of Polymers for Electron Microscopy. *Macromolecules* 1983,16, 589–598.

[32] Ohlsson, B.; Törnell, B.; The Use of RuO₄ in Studies of Polymer Blends by Scanning Electron Microscopy. *J. Appl. Polym. Sci.* 1990, 41, 1189–1196.

[33] Himelfarb, P. B.; Labat, K. B. Characterization of Polymer Blends and Block Copolymers by Conventional and Low Voltage SEM. *Scanning* 1990, 12, 148–154.

[34] Kumar, V.; Suh, N. P. A Process for Making Microcellular Thermoplastic Parts. *Polym. Eng. Sci.* 1990, 30,1323–1329.

[35] Wang, L.; Hikima Y.; Ohshima, M.; Yusa, A.; Yamamoto, S.; Goto, H. Unusual Fabrication of Lightweight Injection-Molded Polypropylene Foams by Using Air as the Novel Foaming Agent. *Ind. Eng. Chem. Res.* 2018, 57, 3800–3804.

[36] Wang, L.; Hikima, Y.; Ishihara, S.; Ohshima, M. Fabrication of High Expansion Microcellular Injection-Molded Polypropylene Foams by Adding Long-Chain Branches. *Ind. Eng. Chem. Res.* 2016, 55, 11970–11982.

[37] Dealy, J. M.; Larson, R. G. *Structure and Rheology of Molten Polymers*; Hanser: Cincinnati, 2006.

[38] Antony, P.; Puskas, J. E. Investigation of the Rheological and Mechanical Properties of a Polystyrene-Polyisobutylene-Polystyrene Triblock Copolymer and Its Blends with Polystyrene. *Polym. Eng. Sci.* 2003, 43, 243–253.

[39] Han, C. D.; Baek, D.M.; Kim, J.K.; Ogawa, T.; Sakamoto, N.; Hashimoto, T. Effect of Volume Fraction on the Order-Disorder Transition in Low Molecular Weight Polystyrene-Block-Polyisoprene Copolymers. 1. Order-Disorder Transition Temperature Determined by Rheological Measurements, *Macromolecules* 1995, 28, 5043–5062.

[40] Han, C. D.; Kim, J.; Kim, J. K. Determination of the Order-Disorder Transition

Temperature of Block Copolymers. *Macromolecules* 1989, 22, 383–394.

[41] Taki, K.; Kitano, D.; Ohshima, M. Effect of Growing Crystalline Phase on Bubble Nucleation in Poly(L-Lactide)/CO₂ Batch Foaming. *Ind. Eng. Chem. Res.* 2011, 50, 6, 3247–3252.

[42] Shaayegan, V.; Wang, G.; Park, C. B. Effect of Foam Processing Parameters on Bubble Nucleation and Growth Dynamics in High-Pressure Foam Injection Molding. *Chem. Eng. Sci.* 2016, 155, 27–37.

[43] Li, D. Y.; Chen, Y. C.; Yao, S.; Zhang, H.; Hu, D. D.; Zhao, L. Insight into the Influence of Properties of Poly (Ethylene-co-octene) with Different Chain Structures on Their Cell Morphology and Dimensional Stability Foamed by Supercritical CO₂. *Polymers* 2021, 13, 1494.